LBL-15085

Conf-820891--3

Lawrence Berkeley Laboratory
UNIVERSITY OF CALIFORNIA

Materials & Molecular
Research Division

LBL--15085

DE83 003662

Presented at the 18th University Series on Ceramic Science Advances in Material Characterization, Alfred University, Alfred, NY, August 16-18, 1982; and to be published in the Proceedings

CROSS-SECTIONAL TRANSMISSION ELECTRON MICROSCOPY OF SEMICONDUCTORS

D.K. Sadana

October 1982

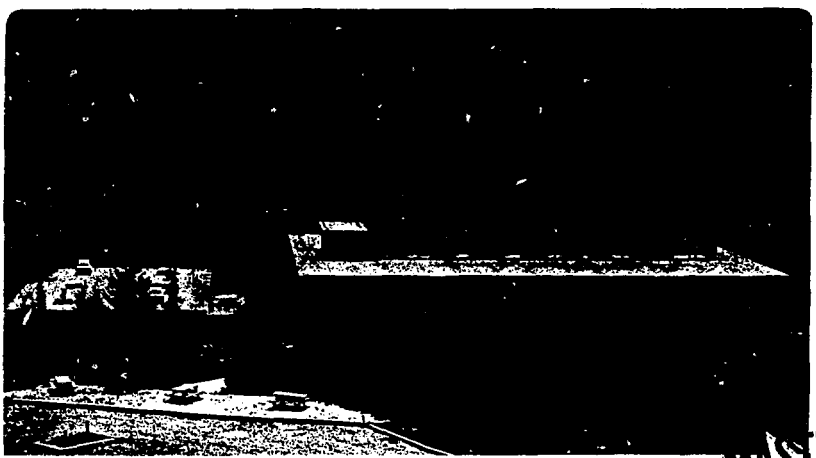

Prepared for the U.S. Department of Energy under Contract DE-AC03-76SF00098

CROSS-SECTIONAL TRANSMISSION ELECTRON MICROSCOPY OF SEMICONDUCTORS

D. K. Sadana

Department of Materials Science and Mineral Engineering
and, Lawrence Berkeley Laboratory
University of California, Berkeley, CA 94720

ABSTRACT

A method to prepare cross-sectional (X) semiconductor specimens for transmission electron microscopy (TEM) has been described. The power and utility of XTEM has been demonstrated. It has been shown that accuracy and interpretation of indirect structural-defects profiling techniques, namely, MeV He^+ channeling and secondary ion mass spectrometry (SIMS) can be greatly enhanced by comparing their results with those obtained by XTEM from the same set of samples.

INTRODUCTION

For a 100 kev transmission electron microscope, the maximum thickness of silicon that can be imaged under the bright-field condition is ~1 micron. Therefore, good quality specimen preparation for TEM studies is one of the essential requirements. The specimens can be prepared in three ways so that either top, edge-on (90° cross-section) or low-angle (1-3°) beveled view of the specimen can be seen. For the top view and low angle beveled view specimens, the thinning is performed by a chemical jet that ejects an $HF:HNO_3$ solution or by low energy (6-10 kev) ion milling. However, for

cross-section type specimens, especially for ion implanted samples where surface layers of thicknesses of only a few 1000 Å are to be viewed, the preparation method involves metchanical thinning followed by ion beam milling.[1] It is nearly impossible to prepare such specimens by chemical thinning. Cross-sectional TEM (XTEM) is a very powerful method because buried damage regions and defects at the sub-surface interfaces can be directly viewed with very high resolution.

PREPARATION TECHNIQUE FOR CROSS-SECTION SPECIMENS

The first stage for specimen preparation is to mechanically prepare a cross-section specimen 25 μm thick. This is schematically illustrated in Fig. 1a. Two pieces of specimen of dimensions 5 mm x 1 mm are glued together face-to-face with contact adhesive, and then mounted on a glass disc with wax with a piece of silicon slice 6 mm x 9mm on either side for support. Then, the surface is polished flat with 240 grit SiC paper followed by another 600 grit SiC paper and 6 μm diamond paste. With some of the III-V compounds, such as InAs, a final 1 μm polish is given to improve the surface finish. Then the specimens are turned over, remounted with wax, and the polishing sequence repeated to give a final specimen less than 25 μm thick.

Subsequent thinning is done by a 6 kV, 50 μA Ar^+ ion-beam. The specimen is mounted with the mechanically polished surface making an angle of ~20° with the ion-beam. It is thinned from one side only at

a time, and the specimen is not rotated. The specimen is orientated with the edge of interest furthest from the ion-beam. After ~1 hr it is turned over and then the other side is thinned until a semi-circular shaped hole occurs at the edge. This procedure preserves the specimen edge without the need for an added protective coating, but occasionally gives rise to some readily recognizable ion beam thinning surface structure. On the other hand, if a protective coating is used, the specimen can be rotated during ion-beam thinning, and such surface structure is markedly reduced.

Figure 2 demonstrates the power and utility of XTEM. In this case, arsenic was implanted at 11 MeV into (100) Si at room temperature and the micrographs were recorded for bright-field conditions. The dark band in Figure 2 a is the image of the amorphous region which is present at a mean depth of 4 microns below the surface. This damage is four times deeper than can be imaged by a conventional 100 keV TEM. The annealing behavior of the damage in Fig. 2a is shown in Fig. 2b. The regrowth features indicate that the solid phase recrystallization proceeds from both upper and lower interfaces. Dislocations remaining after the recrystallization are visible throughout the previously amorphous and partially amorphous regions.

LIMITATIONS

Although room temperature ion beam thinning is used routinely for preparing various types of semiconductor, it has been reported that for some III-V compounds, in particular indium phosphide, cooling the specimens is essential during the thinning.[1]

STRUCTURAL DEFECTS PROFILES FROM XTEM AND OTHER TECHNIQUES

XTEM when combined with indirect structural defect profiling techniques, such as Rutherford backscattering (RBS) in a channeling orientation can greatly enhance the capability of RBS/channeling from merely giving the extent of disorder to characterizing the nature of defects present in the material.[2] This is demonstrated in Fig. 3 where a network of stacking faults appears as a gradually rising dechanneling slope in the channeling spectrum of a 1.6 MeV He^+ beam. The dechanneling from a band of defect clusters (50 Å across) on the other hand has been shown to appear as a broad hump in the channeling spectrum. Dislocation loops produced the least dechanneling.[3]

Comparisons of cross-section TEM images of single and multiple layers of damaged Si with channeled RBS spectra have shown that there is a good qualitative agreement between the damage results from the two techniques. The discrete damage layers as observed by TEM appear as the discrete peaks in the channeled RBS spectra. The mean depths of the damage layers from the two methods also agreed with each other, however, the widths of the damage layers as calculated from the RBS/channeled spectra consistently gave higher values. These comparisons have resulted in improved procedures for determination of damage widths by channeled RBS.[3]

b) TEM/SIMS

Another correlation study is now underway which is expected to enhance the utility of the SIMS technique from its present impurity profiling capability to probing structural defects.[4] In this

case, a fast diffusing impurity which does not react chemically with the semiconductor to be profiled and also is least susceptible to oxidation is used. A good example is Ag in Si. Figure 4 shows the comparison between the Ag profile obtained by SIMS from an Ag implanted (100) Si after annealing at 550°C and the corresponding structural defects profile obtained by XTEM. The conditions for Ag implantation were as follows: 300 keV, RT, 10^{15} cm^{-2}. Before the annealing; the Ag distribution was gaussian and the corresponding XTEM micrograph (not included), showed an amorphous layer extending from the surface to a depth of 2200 Å. However, after annealing at 550°C, the solid phase epitaxial recrystallization occurred at the amorphous/crystalline interface and the interface advanced toward the surface. In addition, a band of fine clusters formed just below the original amorphous/crystalline interface at a mean depth of 2400 Å. The corresponding Ag profile shows that Ag tends to remain in th damaged region only (Fig. 4). The flat Ag distribution extending from the surface to 900 Å correlates precisely with the width of the remaining amorphous region. A small peak in Ag distribution occurs where the band of fine defects is observed. Further experiments on Ag redistribution in the Si samples with other types of defects, such as dislocation loops, line dislocations, polycrystalline regions, etc., indicate that Ag easily segregates locally to the regions containing defects[4] and therefore can be used as a tracer for microdefects in Si.

SUMMARY

1. The preparation method for XTEM specimens has been described.
2. The power and utility of the XTEM has been demonstrated.

3. It has been shown that accuracy and interpretation of indirect structural defects profiling techniques namely, RBS in a channeling oreintation and SIMS can be greatly enhanced by comparing their results with those obtained by XTEM of the same samples.

ACKNOWLEDGEMENTS

The authors would like to thank Peter Byrne of the Electrical Engineering Department of U.C. Berkeley, and Robert Wilson of Hughes Research Labs, Malibu, CA, for providing the specimen of Fig. 2 and SIMS data of Fig. 4, respectively. The financial support for this work came through the Director, Office of Energy Research, Office of Basic Energy Sciences, Materials Research, Division of the U.S. Department of Energy under Contract No. DE AC03-76SF-00098.

REFERENCES

1. J. Fletcher, J. M. Titchmarsh and G. R. Booker, Inst. Phys. Conf. Series (London) 52, 153 (1980).
2. D. K. Sadana, M. Strathman, J. Washburn and G. R. Booker, J. App. Phys. 51, 5718 (1980).
3. D. K. Sadana and J. Washburn, Phys. Rev. B 24 3626 (1981).
4. R. G. Wilson and D. K. Sadana (unpublished).

FIGURE CAPTIONS

Figure 1. A schematic diagram illustrating mechanical polishing: (a) initial mounting of the specimens, (b) after the first side has been polished flat.

Figure 2. Damage distribution obtained by XTEM from an 11 MeV As implanted (100) Si specimen (RT implant), (a) before annealing (b) after two step annealing; 550°C/16 hrs + 945°C/15' in N_2 atmosphere.

Figure 3. 1.6 MeV He^+ dechanneling by stacking faults: (a) Top view bright-field TEM microraph showing stacking faults, (b) depth distribution of stacking faults in the specimen (a), and (c) channeling spectrum from the same specimen. Experimental conditions; $P^+ \longrightarrow$ (111) Si, $10^{15} cm^{-2}$, 120 keV, Q switched ruby laser annealed at 1.2J cm^{-2}.

Figure 4. Ag segregation to defects rich regions in (100) Si: (a) bright-field XTEM micrograph, (b) Ag depth distribution from SIMS. Experimental conditons: Ag $\longrightarrow$ (100) Si, $10^{15} cm^{-2}$, RT; annealed at 550°C for 15 minutes.

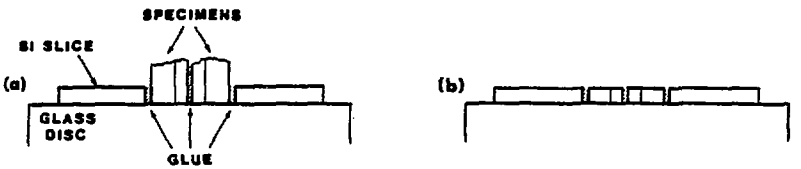

XBL 823-8451

Fig. 1

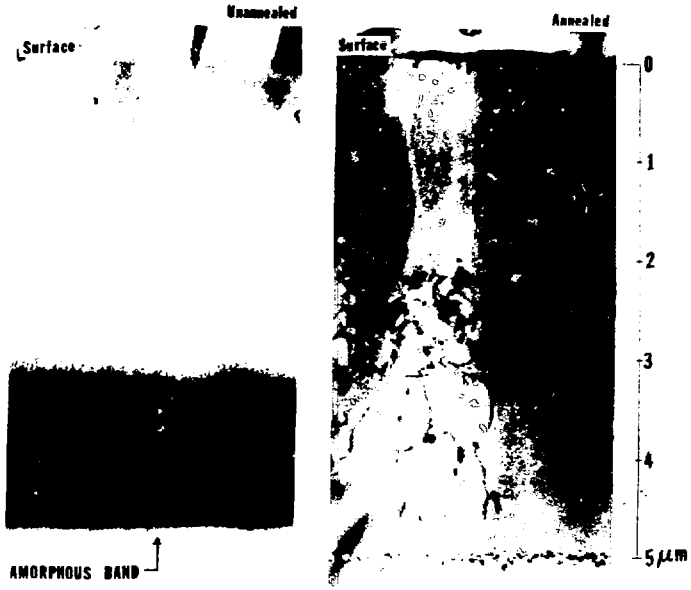

a b

XBB 825-4385

Fig. 2

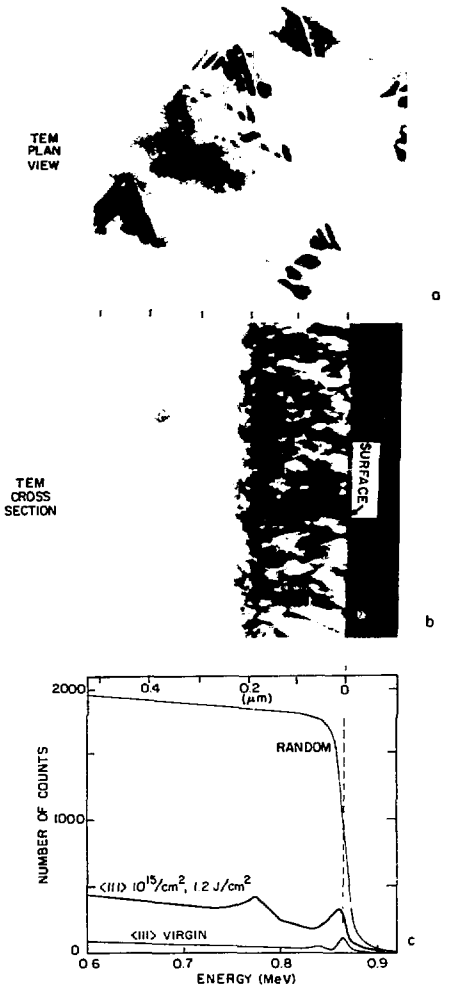

XBB 813-2733

Fig. 3

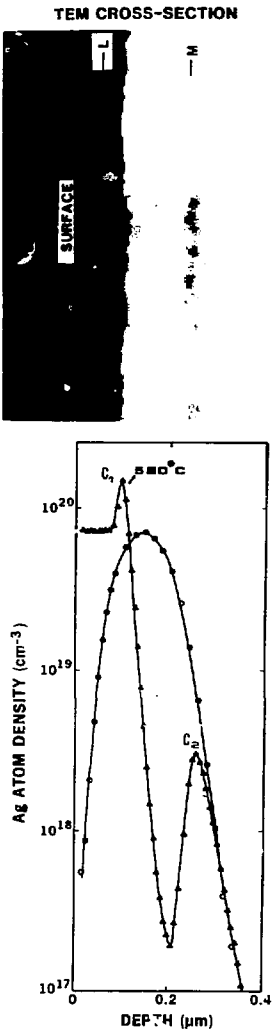

XBB 810-9936

Fig. 4